Progress In Electromagnetics Research, Vol. 121, 535–555, 2011

AUTOMATED SAR REFERENCE IMAGE PREPARATION FOR NAVIGATION

S. Ren*, W. Chang, T. Jin, and Z. Wang

School of Electronic Science and Engineering, National University of Defense Technology, Changsha 410073, P. R. China

Abstract—The preparation of good navigational synthetic aperture radar (SAR) reference image is critical to the SAR scene matching aided navigation system, especially for complex terrain. However, few papers discuss the problem, and almost none of the methods proposed by them are fully automatic. Based on the practical requirements, a fully automated method of SAR reference image preparation is introduced. Firstly, a number of distinctive control points (CP) in the simulated SAR image is detected based on a method of image segmentation and clustering. Then, the corresponding tie-points in the real SAR image are searched based on local similarity by means of template matching. To improve the accuracy of CP, a method for segmentation threshold calculation, outlier screening and sub-pixel location computation is presented. Finally, the real SAR image is warped to the simulated one, and then projected to the frame of digital elevation model (DEM) by the polynomial mapping function. Experimental results on real data sets demonstrate the accuracy and efficiency of the proposed method.

1. INTRODUCTION

The inertial navigation system (INS)/synthetic aperture radar (SAR) navigation system, which makes use of SAR technology, not only has all-weather and all-day capabilities, but also increases the capabilities of interference suppression. The navigation system matches the real-time image and a geo-referenced image (also called reference image) to obtain the position update information, and corrects the cumulated error of INS by fusing the update information with INS measurements [1]. The accuracy of reference image affects the

Received 14 September 2011, Accepted 26 October 2011, Scheduled 5 November 2011
* Corresponding author: Sanhai Ren (sanhairen@163.com).

performance of scene matching, and plays an important role on the final accuracy of navigation.

In the early days, since it is convenient and accessible to acquire optical images of interested regions, the INS/SAR navigation system generally takes optical image as reference image. However, the tremendous differences between optical image and SAR image increase the difficulty of scene matching, and even decrease the accuracy of navigation. In order to increase the similarity between reference image and real-time image, and improve the accuracy of navigation, it is a trend to take SAR image as reference image. It is a pity that few technologies of SAR reference image preparation are available from the open literature. According to the principles of scene matching navigation [1], this paper prepares SAR reference image by means of geometric correction.

The geometric correction method, based on whether it takes use of control points (CP), can be divided into two main categories: the method based on imaging model [2–5] and the method based on SAR image simulation [6–8].

The first method, which corrects geometric distortions mainly by constructing imaging model (such as polynomial model, Konenecy model, Leberl model and R-D model), can receive high accuracy if some accurate CPs or precise state vectors of SAR can be provided in advance. However, the accuracy of the method will decrease greatly under some mountainous terrains, since it is difficult to detect CPs under these areas. The second method, which corrects geometric distortions mainly by the matching of real and simulated SAR image, can get rid of the requirements of CPs and state vectors. Therefore, the second method becomes the preferred one to correct SAR images of mountainous regions. The research of this paper is based on it.

For the correction method based on SAR image simulation, the critical step is the CP detection and matching. The CPs are the distinctive points in the image, which can be easily recognized and detected. The more precise of the CPs, the more accurate geometric accuracy will be got. Therefore, various methods for CP detection are developed taking into account the different characteristics of image data. Liu et al. [7] proposes a method of CP detection using image processing soft. The method first detects CPs in the simulated SAR image via image processing soft, then searches the tie-points in the real SAR image by image matching. Sheng and Alsdorf [6] and Bentoutou et al. [9] suggest an edge-based method of CP detection, which does the edge detection firstly, and then detects CPs in the edge image using corner detector. Though these methods can detect a set of reliable CPs, they don't take into account the characters of SAR image

under mountainous areas, where the features of layover and shadow are obvious. Therefore, the performance of these methods will decrease when they are used in the mountainous SAR images. Some researches taking layover and shadows as features for CP detection are carried out by [4, 10, 11]. However, the aim of [4] is to provide support to a human operator in an interactive procedure, but not to develop a fully automated system. The method proposed in [10] dose not give the detailed description of the method. The method developed by [11] just completes some experiments on the factors which affect the matching of real and simulated image, but no accuracy evaluation of the CPs is given.

Aims at researching on fully automated method of reference image preparation for navigation, a new method for control point detection and matching is proposed in this paper. Firstly, CPs in the simulated SAR image are detected by an improved gray segmentation and clustering method. Then, for each CP, the corresponding tie-point in the real SAR image is searched based on the image offset and local similarity by template matching. In the end, the real SAR image is registered to the simulated one by using polynomial interpolation, and then projected to the DEM map based on the imaging geometry. In order to improve the accuracy of the method, some improved methods are introduced, which improves the geometric accuracy of the reference image.

This paper is organized as follows. The proposed method of reference image preparation is described in Section 2, which mainly deals with the CP detection and CP matching. Results of experiments on real data sets are reported in Section 3. Finally, the related conclusions are given in Section 4.

2. THE METHOD OF REFERENCE IMAGE PREPARATION

Typical SAR image of mountainous terrain is illustrated in Figure 1, which is in an area around (105.8371°E, 26.1098°N). The elevations of the imaging area range from 1110 m to 1530 m. From Figure 1 we can see that there exist severe geometric distortions in the SAR image, such as layover, shadow and foreshortening. If such images are used in image matching, the matching probability and accuracy will decrease [12, 13]. Therefore, INS/SAR navigation system always takes geometrically rectified SAR image as reference image.

Typical procedures involved in the correction method based on image simulation are as follows: (1) rotating DEM according to the azimuth angle, so that the north of DEM will be consistent with the

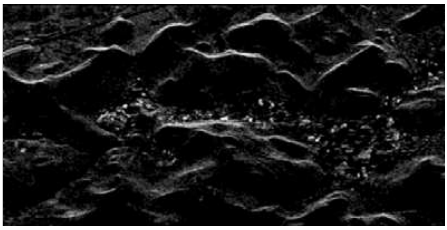

Figure 1. SAR image of mountainous region. The horizontal is the azimuth direction, and the vertical is the range direction, hereinafter the same.

direction of flight; (2) simulating a SAR image from DEM according to the imaging geometry of the real SAR image; (3) detecting reliable tie-points (TPs) that appear in both the real and simulated SAR image; (4) warping the real SAR image to the simulated one using a appropriate mapping function; (5) projecting the warped real SAR image back to the DEM map using the imaging relationship. The general flow chart of the proposed method is shown in Figure 2.

The method requires two types of inputs: DEM data and the real SAR image, where the latter one includes some imaging parameters, such as sensor altitude H, incidence angle θ and azimuth angle η. H is used in slant range calculation and geometric distortion simulation from DEM, θ is used in backscatter amplitude calculation, and η is used in DEM rotation. In some operational case, if the real SAR image isn't at Zero-Doppler, the velocity of the aircraft is needed, too.

According to the grid space of DEM and the pixel size of real SAR image, the DEM data is interpolated [14] or the SAR image is re-sampled to decrease the scale difference between real and simulated SAR image. Then, SAR image and layover image are simulated from DEM based on the facet model [15] and the geometric relationship of the real SAR image (which is called lookup table in this paper) [16].

The critical steps of the proposed method are CP detection and CP matching. The CP detection is implemented by an effective image segmentation and clustering method. The CP matching is implemented in two stages for accuracy. The first-stage CP matching is only implemented for the transformation parameters calculation, and it requires an input of the preprocessed real and simulated SAR image, and the range offset between them. The detected tie-points and calculated transformation parameters in the first-stage are inputted into the stage-2 CP matching for outlier screening to produce the final set of tie-points with high accuracy.

In the end, the real SAR image is warped to the simulated one

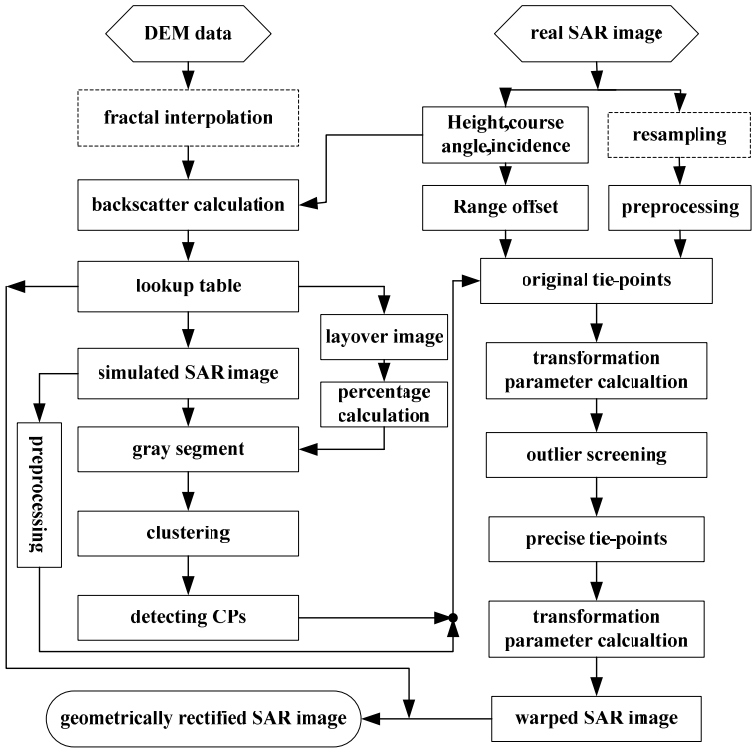

Figure 2. The flow chart of reference image preparation, where the dashed frames are optional processes.

and then projected to the DEM map using the final set of tie-points by a polynomial mapping function.

The output of the above procedures is a geometrically rectified SAR image with geometric and topographic distortions removed.

2.1. Control Point Detection

2.1.1. SAR Image Simulation

There are two main parts included in the SAR image simulation: 1) backscatter modeling; 2) coordinate transformation. The purpose of SAR image simulation is to acquire tie-points through the image matching between real and simulated SAR image. The key point is to create a SAR image that is similar or identical in geometry with the real SAR image. Therefore, the backscatter modeling doses not require

a simulated SAR image that has absolutely correct backscatter values. The typical backscattering model is cosine model, which includes three types [17],

$$\begin{aligned} &\text{Model 1:} \quad \rho = \sqrt{\cos\theta} \\ &\text{Model 2:} \quad \rho = \cos\theta \\ &\text{Model 3:} \quad \rho = 90 - \theta \end{aligned} \tag{1}$$

where ρ is the backscattered amplitude, θ is the local incidence angel presented in degree. Considering backscattered power of these three models, it is found that Model 2 assumes a Lambert's law surface, which is more suitable for backscattered amplitude calculation.

SAR imaging geometry is shown in Figure 3(a), where the black dashed frame is the original DEM, and the overstriking black frame is the rotated DEM. If the earth curvature can not be ignored, the Range-Doppler (RD) method is the preferred imaging model, which accurately describes the relationships between slant range and Doppler via three equations. However, Rees and Steel [18] compared three earth models at various levels of simplification, and showed that the flat earth simplification is a reasonable, efficient and sufficiently accurate

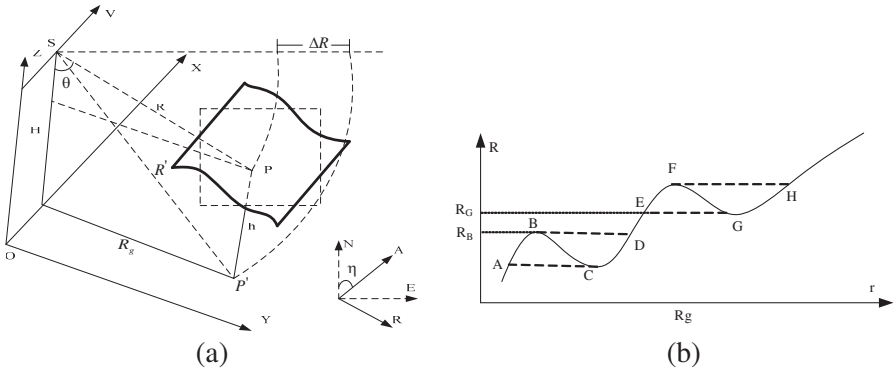

Figure 3. Geometry of topographical distortions in SAR imagery. (a) is the imaging geometry of SAR. Under the assumption of flat earth surface, the datum plane is a horizontal surface. H is sensor altitude, θ is incidence angle, η is azimuth angle, h is the elevation of target P, P' is the vertical projection of P on the datum plane, R is the slant range between target P and sensor, R' is the slant range between P' and sensor, R_g is the ground range of P, ΔR is the slant range offset induced by elevation h. The coordinate system N-E is an east-north-up system, A-R is an azimuth-range system, O-XYZ is a Cartesian system. (b) is the amplitude of slant ranges along a range line.

approximation. Therefore, a simple method to construct the lookup table is proposed in this paper. From Figure 3(a), we have the following expression for the slant range of target P:

$$R = \sqrt{(H-h)^2 + R_g^2} = \sqrt{(H-h)^2 + (R_{g\min} + (n-1)\cdot S_p)^2} \quad (2)$$

where R_g is the ground range of target P, $R_{g\min}$ is the nearest ground range, n is the range coordinate of P in the DEM, S_p is the grid space of DEM, H is the sensor altitude, and h is the elevation of P.

Firstly, the slant range R is compared with the slant range sequence of SAR image.

$$D_{if}(m) = R - S_r(m) = R - [S_{rn} + (m-1)\cdot d_r] \quad (3)$$

where S_{rn} is the nearest slant range, d_r is the pixel size of range, m is the range coordinate of SAR image. Then, the location with least difference is searched, and taken as the corresponding location of P in the simulated image. Finally, the backscattered amplitude of P is added to that of the corresponding position in the simulated image. When all the targets in DEM are processed, the SAR image simulation is completed.

In this paper, $H = 4\,\text{km}$, $\theta = 44^\circ$, and $\eta = 180^\circ$ are used as the nominal sensor parameters in SAR image simulation. The simulated SAR image is shown in Figure 4(a), from which we can see that the simulated SAR image is similar with the real SAR image in geometry.

For the convenience of following description, the method of layover image simulation is presented [16]. In order to search for all the layover regions, the method is divided into two steps: along each range line, (1) Searching from near to far, and find the first maximum (as B illustrated in Figure 3(b), whose slant range is R_{B}). Then, taking B as the origin, search the slant range until the slant range increases to R_{B} again (as D illustrated in Figure 3(b)), and label all the points in this scope

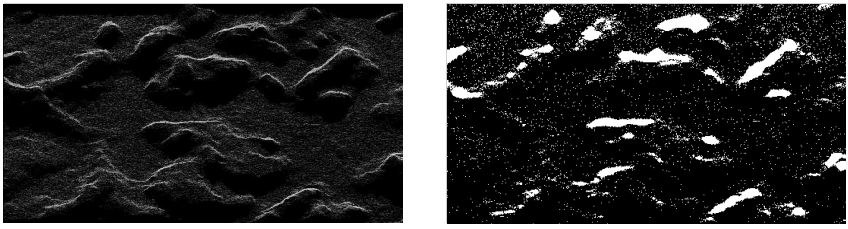

(a) (b)

Figure 4. Simulated image. (a) is the simulated SAR image. (b) is the layover image in the DEM coordinate system, where the white points are layover points.

as layover points. Next, search other layover points using the same method until the farthest slant range; (2) Searching from far to near, and find the first minimum (as G illustrated in Figure 3(b), whose slant range is R_{G}). Then, taking G as the origin, search the slant range until the slant range decreases to R_{G} again (as E illustrated in Figure 3(b)), and label all the points in this scope as layover points. Next, search other layover points using the same method until the nearest slant range.

From the above procedures, we can get that the points in the scope A-D and E-H in Figure 3(b) are all layover points, where B-C and F-G are active layover regions, and the others are passive layover regions. The simulated layover image is shown in Figure 4(b).

2.1.2. Image Segmentation

The general object of image segmentation is to separate the interested regions out of the image. The segmented image replaces the pixels, whose gray value greater than the threshold, with the value 1 (white), and replaces all other pixels with the value 0 (black). The threshold, which is specified in the range of [0, 1], is a crucial factor in the segmentation. Some methods to determine the gray threshold are proposed in [19, 20], such as histogram-based method, otsu-based method and watershed-based method. However, since none of the methods consider the characters of layover regions in the simulated image, they are ineffective in the layover region segmentation. A simple method of gray threshold calculation is introduced, as described follows:

(1) Simulate a layover image in slant range plane based on the method presented in Section 2.1.1, and calculate the percentage of the layover pixels in the layover image, denoted by R_{io}.
(2) Quantify the simulated SAR image to 8 bits, and calculate the histogram.
(3) Sum the pixels in each level of the histogram until the percentage of the summation to the total pixels equals to $1 - R_{io}$, and save the current level of the histogram.
(4) Take the ratio of the current level to the maximal level as the gray threshold. The maximal level is 256 for the images of 8 bits.

Figure 5 demonstrates the segmentation results using the Otsu and the proposed method. Although the method based on Otsu can segment the layover region too, the results include non-layover regions (as Figure 5(a) shows), which will burden the following CP detection. The proposed method can segment the connected layover regions only (as Figure 5(b) shows), assisting the following CP detection.

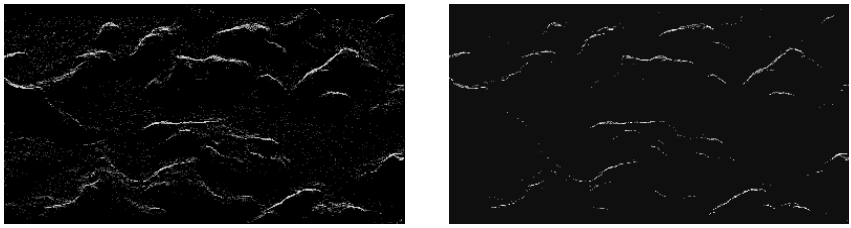

(a) (b)

Figure 5. The segmentation results. (a) is the segmentation result using the threshold determined by Otsu. (b) is the segmentation result using the threshold calculated by the proposed method.

2.1.3. Control Point Detection

An improved clustering method is selected to detect CP based on the special characters of SAR image under mountainous terrains, where the features of layover and shadow are obvious.

For the 0-1 binary image from image segmentation or the mask image (created by multiplying the 0-1 binary image by the original image), the function of clustering is to assemble the points within a range, and acquire a new clustering center.

Suppose that the mask image ($M \times N$ pixels) is $\mathbf{A} = \{a_{ij}\}$, where $i = 1, 2, \ldots, M$, $j = 1, 2, \ldots, N$, and the range threshold judging whether two pixels belong to the same region is D (which is also called clustering radius). Then, the flow of CP detection is as follows:

(1) Read each pixel a_{ij} according to its order in the row and column. If $a_{ij} = 0$, read the next pixel; or else, go to the next step.

(2) Calculate the range $\{d_1, d_2, \ldots, d_L\}$ between a_{ij} and the already saved clustering center $\{[x_1, y_1, k_1], [x_2, y_2, k_2], \ldots, [x_L, y_L, k_L]\}$ ($[x_L,\ y_L]$ is the coordinate of the clustering center, k_L is the number that the clustering center has clustered, L is the number of clustering centers). If $L = 0$, or $d_1, d_2, \ldots, d_L > D$, save the a_{ij} as a new clustering center, i.e., $x_1 = i$, $y_1 = j$, or $x_{L+1} = i$, $y_{L+1} = j$; or else, given $R_d = \{d_1, d_2, \ldots, d_L\}$, if there is a subset $S = \{\, s | \, s \in R_d \ \&\ s \leq D\}$, picking the qth clustering center who clusters the least pixels, and go to the next step.

(3) Perform the following process to the qth clustering center:

$$k'_q = k_q + 1 + a_{i,j} / \max(a_{i,j}) \tag{4}$$

$$x'_q = \frac{1}{k'_q} \left(x_q \times k_q + i \cdot [a_{i,j} / \max(a_{i,j})] \right) \tag{5}$$

$$y'_q = \frac{1}{k'_q}\left(y_q \times k_q + j \cdot [a_{i,j}/\max(a_{i,j})]\right) \tag{6}$$

Then, we can get the updated value of the qth clustering center after a_{ij} added in.

(4) When all the pixels in **A** are processed, screen out the clustering centers whose k_L are less than the number threshold N_T, and the centers whose $[x_L, y_L]$ are too close to the boundary of the image (i.e., the distance between $[x_L, y_L]$ and the boundary of the image is smaller than the distance threshold D_T). Then, save the remainder as CPs.

From the above procedures, a dense set of CPs can be detected. If the layover region distributes all over the image, then the CPs will distribute all over the image too. Figure 6 illustrates the CPs detected in the simulated image, from which we can see that the detected CPs distribute along layover regions.

2.2. The Image Offset Calculation

If the image offset between real and simulated SAR image can be got in advance, the process of CP matching will be speeded up. However, the general methods to acquire the offset are by visually comparing the image pairs [6, 9], which need human intervention. An automated method of image offset calculation is proposed in this paper.

From Equation (2), the slant range error induced by parameter errors can be calculated as:

$$\Delta R_H = \frac{\partial R}{\partial H}\Delta H = \frac{H-h}{\sqrt{(H-h)^2 + R_g^2}}\Delta H = \Delta H \cdot \cos\theta \tag{7}$$

$$\Delta R_h = \frac{\partial R}{\partial h}\Delta h = \frac{-(H-h)}{\sqrt{(H-h)^2 + R_g^2}}\Delta h = -\Delta h \cdot \cos\theta \tag{8}$$

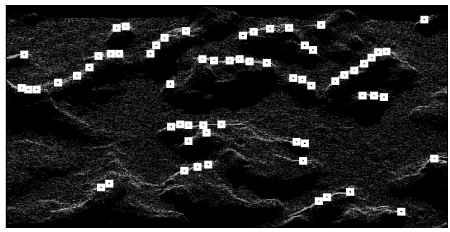

Figure 6. The CPs detected in the simulated SAR image. The white frames are detected CPs.

$$\Delta R_{gr} = \frac{\partial R}{\partial R_g}\Delta gr = \frac{R_g}{\sqrt{(H-h)^2 + R_g^2}}\Delta gr = \Delta gr \cdot \sin\theta \tag{9}$$

$$\Delta R_\theta = \frac{\partial R}{\partial R_g}\frac{\partial R_g}{\partial \theta}\Delta\theta = \frac{R_g}{\sqrt{(H-h)^2 + R_g^2}} S_{rn} \cdot \cos\theta \cdot \Delta\theta$$

$$= \frac{S_{rn}}{2} \cdot \sin(2\theta) \cdot \Delta\theta \tag{10}$$

where ΔH, Δh, Δgr, and $\Delta\theta$ are sensor altitude error, DEM elevation error, ground range error and incidence angle error, respectively, ΔR_H, ΔR_h, ΔR_{gr}, and ΔR_θ are the corresponding slant range error, S_{rn} is the nearest slant range. Given the location accuracy of GPS in longitude and latitude are (Δa, Δr), then the azimuth error and ground range error induced by them are:

$$\Delta A = \Delta a \cdot \cos\eta + \Delta r \cdot \sin\eta \tag{11}$$

$$\Delta gr = -\Delta a \cdot \sin\eta + \Delta r \cdot \cos\eta \tag{12}$$

If the pixel size is $d_a \times d_r$ (azimuth $\times$ range), we can get the image offset (ΔA, ΔR) in pixel:

$$\Delta A = \Delta A / d_a \tag{13}$$

$$\Delta R = \left(\Delta R_H + \Delta R_h + \Delta R_{gr} + \Delta R_\theta\right) / d_r \tag{14}$$

Since small angle errors have little influence on cosine value and sine value, the incidence angle used in (7)–(12) can be the defined value in the SAR image simulation. Otherwise, since the range measure is accurate for SAR, the S_{rn} can be assumed fully accurate.

2.3. Control Point Matching

CP matching is one of the most important tasks in automated image rectification. However, the severe speckle noise and quantization noise in real SAR image decreases the performance of CP matching. Some preprocessing should be implemented before matching. By comparing the results of general used methods for speckle suppression, such as multi-look processing, median filter, smoothing filter, Lee filter and enhanced Lee filter, Gamma MAP filter and enhanced Gamma MAP filter [21], the enhanced Lee filter is considered as the best method for speckle suppression. For the quantization noise, it can be suppressed by setting the minimal gray threshold. Furthermore, in order to increase the radiometric quality of the simulated SAR image, it can be calibrated by matching its histogram to that of the real SAR image.

Based on the image offset and the CPs detected in the simulated SAR image, the tie-points in the real SAR image can be derived

by some similarity measures, such as correlation coefficient, gray mean square difference, gray standard difference, invariant moments and Hausdorff distance. Normalized correlation coefficient (NCORR) is selected as the similarity measure in this paper since it is computationally straightforward and normalized to the range of -1 to 1. In addition, the measure is not affected by scalar multiplication or addition of a constant to one of the images, making it immune to many artifacts introduced into images by sensors and simulation [6]. In order to speed up the CP matching, correlation computation is limited within the image offset. The tie-points in the real SAR image are determined as follows.

(1) For every control point (x_{ref}, y_{ref}) in the simulated SAR image, choose a circular template W_1 of radius R_{ad} centered at this point.

(2) Find the candidate tie-point in the real SAR image via the image offset, and determine a search region around the tie-point. Calculate the NCORR of W_1 and the corresponding template W_2 centered at each point in the search region. When every point in the search region is processed, find the location (x_{rel}, y_{rel}) with the maximal coefficient ρ_m. If $\rho_m > G_T$ (G_T is the threshold), save (x_{rel}, y_{rel}) as the corresponding tie-point of (x_{ref}, y_{ref}), or else screen out (x_{ref}, y_{ref}).

(3) From (1) and (2), we can get a set of tie-points. Although some tie-points pass the CP matching, they may still be problematic and appear as outliers showing offsets significantly different from their surrounding tie-points. These outliers need to be removed. A method is developed to screen out outliers. Based on the tie-points and polynomial interpolation model described in the following section, the transformation parameters are estimated and all the CPs in the real SAR image are transformed into the simulated image. Given CPs in the simulated SAR image are (x_{ref_i}, y_{ref_i}), and CPs transformed from the real SAR image are (x'_{ref_i}, y'_{ref_i}), $i = 1, 2, \ldots, M$, where M is the number of tie-points. Then, the distance between them can be calculated as:

$$E_{rror} = \sqrt{\left(x_{ref\_i} - x'_{ref\_i}\right)^2 + \left(y_{ref\_i} - y'_{ref\_i}\right)^2} \tag{15}$$

If the distance is bigger than the threshold E_T, the corresponding CP is screened out as outlier.

(4) The tie-points after outlier screening are saved to calculate the transformation parameters and validate the accuracy of the method.

In order to improve the accuracy of CP matching, it is necessary to provide methods to obtain sub-pixel precision, because the described

CP matching approach only determines CPs up to integer accuracy. Several approaches have been proposed to obtain sub-pixel accuracy in CP matching, such as analytical matching interpolation methods [22] and image-interpolation methods [23]. Since the image interpolation approach is computationally expensive compared to the analytical match-interpolation method [9], the analytical match-interpolation method is used in this paper. In this case, sub-pixel accuracy is achieved by interpolating in the match measure surface to estimate the position of the peak. Given the discrete match measure surface $S(a, r)$ and the best match position (a_0, r_0), the estimated coordinates (a, r) of the match peak around (a_0, r_0) are calculated as

$$a = a_0 - \frac{1}{2} + \frac{S(a_0, r_0) - S(a_0 - 1, r_0)}{2S(a_0, r_0) - S(a_0 - 1, r_0) - S(a_0 + 1, r_0)} \quad (16)$$

$$r = r_0 - \frac{1}{2} + \frac{S(a_0, r_0) - S(a_0, r_0 - 1)}{2S(a_0, r_0) - S(a_0, r_0 - 1) - S(a_0, r_0 + 1)} \quad (17)$$

The CPs after outlier screening in the simulated SAR image are illustrated in Figure 7(a). The tie-points derived in the real SAR image are illustrated in Figure 7(b). From Figure 7, we can get that the more severe of the layover is, the more CPs will be detected, and enough tie-points can be detected via the proposed method.

2.4. Image Warping and Geometric Rectification

With the derived tie-points, the real SAR image can be warped into the simulated SAR image by applying a mapping function. The general used mapping function models include: affine model, polynomial model, B-splines function model, tine-plate spline function model, and piecewise deformation model. Since the image in this paper is only a

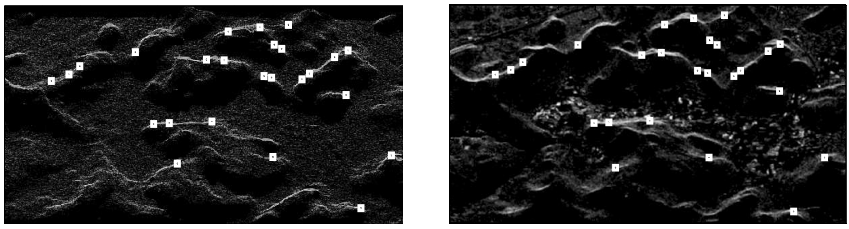

(a) (b)

Figure 7. The tie-points in the simulated and real SAR image. (a) illustrates the CPs after outlier screening in the simulated SAR image. (b) illustrates the tie-points corresponding to the CPs in (a). The white frames are CPs.

portion of the SAR image, and the geometric features in the simulated and real SAR image are consistent, the bilinear polynomial model is selected as the mapping model. If the image to register is a huge one or more complex, the more complicated polynomial model should be selected. Even the B-splines model and piecewise deformation model should be selected.

Given the CPs in the simulated SAR image are (x_{ref_m}, y_{ref_m}), and the corresponding tie-points in the real SAR image are (x_{rel_m}, y_{rel_m}) ($m = 1, 2, \ldots, N$, where N is the number of CPs after outlier screening), the polynomial function model between two images can be expressed as:

$$\begin{aligned} h(x_{ref}) &= a_1 + a_2 \cdot x_{rel} + a_3 \cdot y_{rel} + a_4 \cdot x_{rel} \cdot y_{rel} \\ h(y_{ref}) &= b_1 + b_2 \cdot x_{rel} + b_3 \cdot y_{rel} + b_4 \cdot x_{rel} \cdot y_{rel} \end{aligned} \tag{18}$$

In order to solve for the transformation parameters, the equation above can be rewritten to gather the unknowns into a column vector:

$$\begin{bmatrix} x_{ref\_1} \\ y_{ref\_1} \\ \vdots \\ x_{ref\_N} \\ y_{ref\_N} \end{bmatrix} = \begin{bmatrix} 1 & 0 & x_{rel\_1} & 0 & y_{rel\_1} & 0 & x_{rel\_1} \cdot y_{rel\_1} & 0 \\ 0 & 1 & 0 & x_{rel\_1} & 0 & y_{rel\_1} & 0 & x_{rel\_1} \cdot y_{rel\_1} \\ & \vdots & & & & \vdots & & \vdots \\ 1 & 0 & x_{ref\_N} & 0 & y_{ref\_N} & 0 & x_{ref\_N} \cdot y_{ref\_N} & 0 \\ 0 & 1 & 0 & x_{ref\_N} & 0 & y_{ref\_N} & 0 & x_{ref\_N} \cdot y_{ref\_N} \end{bmatrix} \begin{bmatrix} a_1 \\ b_1 \\ \vdots \\ a_4 \\ b_4 \end{bmatrix} \tag{19}$$

Let $\mathbf{A} = \begin{bmatrix} x_{ref\_1} \\ y_{ref\_1} \\ \vdots \\ x_{ref\_N} \\ y_{ref\_N} \end{bmatrix}$, $\mathbf{H} = \begin{bmatrix} 1 & 0 & x_{rel\_1} & 0 & y_{rel\_1} & 0 & x_{rel\_1} \cdot y_{rel\_1} \\ 0 & 1 & 0 & x_{rel\_1} & 0 & y_{rel\_1} & 0 \\ & \vdots & & & & \vdots & \\ 1 & 0 & x_{ref\_N} & 0 & y_{ref\_N} & 0 & x_{ref\_N} \cdot y_{ref\_N} \\ 0 & 1 & 0 & x_{ref\_N} & 0 & y_{ref\_N} & 0 \end{bmatrix}$

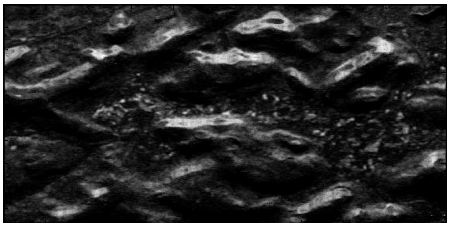

Figure 8. The geometrically corrected SAR image.

$$\begin{bmatrix} 0 \\ x_{rel\_1} \cdot y_{rel\_1} \\ \vdots \\ 0 \\ x_{ref\_N} \cdot y_{ref\_N} \end{bmatrix}, \mathbf{P} = \begin{bmatrix} a_1 \\ b_1 \\ \vdots \\ a_4 \\ b_4 \end{bmatrix}, \text{ we can write this linear system as}$$

$$\mathbf{HP} = \mathbf{A} \tag{20}$$

Then the least-square solution for the parameter vector $\mathbf{P}$ can be determined by solving the corresponding normal equations

$$\mathbf{P} = \left[\mathbf{H}^T\mathbf{H}\right]^{-1}\mathbf{H}^T\mathbf{A} \tag{21}$$

Then the real SAR image can be warped into the simulated SAR image, and projected to the DEM map by the lookup table.

The result of the above procedures is a geometrically corrected SAR image, as Figure 8 shows, from which we can see that the geometric distortions of layover and foreshortening are all removed. However, the shadow can not be removed by the proposed method. The interested readers can find the method to compensate shadow in [24].

3. EXPERIMENTAL RESULTS AND ANALYSIS

The procedures proposed in Section 2 were implemented in MATLAB, on a 2.4-GHz processor Windows platform with 2 GB physical memory. The selected real SAR image, which is acquired on July 2010, is in an area around (105.8371°E, 26.1098°N). The size of the image is 4000×5430 pixels, and the pixel size is $0.5\,\text{m} \times 0.5\,\text{m}$. The azimuth angle is about 180°, which means the heading of the flight is from north to south. Based on the GPS/INS measure, we find the corresponding DEM, whose elevation ranges from 1110 m–1530 m, and grid space is $20\,\text{m} \times 20\,\text{m}$. Considering there is a huge discrepancy between pixel size and grid space, which is about 40 times, the DEM and SAR image are processed at the same time. The final pixel size of the image and

the grid space of DEM are both 2.5 m × 2.5 m. The final SAR image is illustrated in Figure 1.

Based on the experiments and analysis, the parameters used in the proposed method are determined as follows:

(1) According to the typical parameter errors, such as $\Delta H \approx 10\,\text{m}$, $\Delta h \approx 7\,\text{m}$, $\Delta gr \in [-30\,\text{m}, 30\,\text{m}]$, and $\Delta\theta \approx -2^\circ$, the offset between real and simulated SAR image were determined to be $(-102, 25)$ m [about $(-40, 10)$ pixels] in the range direction (i.e., west-east), and $(-30, 30)$ m [about $(-12, 12)$ pixels] in the azimuth direction (i.e., north-south).

(2) The clustering radius and the threshold of clustered numbers in the clustering method determine the number of CP. The smaller of the clustering radius, and the lower of the threshold, the more CPs will be detected. Otherwise, the estimated parameters will be more sensitive to position errors if the CPs are too close to each other. Therefore, the clustering radius $D = 30$, the threshold of the clustered numbers $N_T = 30$, and distance threshold $D_T = 20$, are used in this paper.

(3) The template radius R_{ad} is a very important factor in the CP matching. In order to reduce the computation time to a minimum, this template should be as small as possible. However, the size of the template determines the amount of statistical information that is provided. Small templates will yield unreliable match values. Experiments in this work indicate that a template of radius being 15 yields a good compromise between computational speed and statistical reliability. Otherwise, the NCORR threshold $G_T = 0.6$, and outlier screening threshold $E_T = 3$ is used in this paper based on experiments.

In order to validate the accuracy of the method, parts of the tie-points are employed to estimate the transformation parameters, and the others are used as checkpoints. For a quantitative error analysis, the mean error, the maximum error, and the root mean square error (RMSE) are always computed from these checkpoints [18]. RMSE error, which is more statistically meaningful, is commonly used in error evaluation. According to the polynomial mapping model (as (18) shows), the CPs in the real SAR image can be mapped into the simulated SAR image as follows:

$$\begin{aligned} x'_{ref\_i} &= [1\ x_{rel\_i}\ y_{rel\_i}\ x_{rel\_i} \cdot y_{rel\_i}] \cdot [a_1\ a_2\ a_3\ a_4]^T \\ y'_{ref\_i} &= [1\ x_{rel\_i}\ y_{rel\_i}\ x_{rel\_i} \cdot y_{rel\_i}] \cdot [b_1\ b_2\ b_3\ b_4]^T \end{aligned} \tag{22}$$

where $i = 1, 2, \ldots, N_V$, and N_V is the number of checkpoints. Then

Table 1. The coordinates of checkpoints in (azimuth, range).

CP	Simulated SAR image	Real SAR image	CP	Simulated SAR image	Real SAR image
1	(769, 929)	(766.73, 941.44)	6	(577, 699)	(567.98, 710.76)
2	(451, 388)	(440.81, 394.80)	7	(282, 774)	(265.31, 778.30)
3	(441, 540)	(429.96, 547.49)	8	(276, 696)	(255.41, 706.54)
4	(446, 429)	(436.18, 435.75)	9	(288, 121)	(259.46, 124.03)
5	(280, 146)	(252.81, 147.69)	10	(85, 666)	(52.39, 668.54)

Table 2. The RMSE of checkpoints (in pixel).

CP	1	2	3	4	5	6
RMSE	0.34	0.74	0.42	0.85	0.98	0.88
TGM	\	\	\	\	\	\
EBM	\	\	\	\	\	\
CP	7	8	9	10	Total	Time
RMSE	1.05	1.21	1.3	2.02	0.979	15 min
TGM	\	\	\	\	2.143	100 min
EBM	\	\	\	\	1.451	30 min

the RMSE can be calculated as:

$$\text{RMSE} = \sqrt{\frac{\sum_{i=1}^{N_V}\left(\left(x_{ref\_i} - x'_{ref\_i}\right)^2 + \left(y_{ref\_i} - y'_{ref\_i}\right)^2\right)}{N_V}} \tag{23}$$

In the end, ten checkpoints are selected to compute the RMSE. The coordinates of these checkpoints are illustrated in Table 1. The coordinates in the real SAR image are in sub-pixel, which are calculated from (16) and (17). From Table 1, we can see that the checkpoints distribute all over the image.

The estimated RMSE of ten checkpoints is listed in Table 2, from which we know that the total RMSE is about one pixel (i.e., 2.5 m). According to the incidence angle, the RMSE will be 3.599 m in the ground range plane. Suppose the DEM is accurate, the accuracy of the reference image is 3.599 m.

As mentioned in Section 2, the sensor parameters (i.e., sensor altitude, incidence angle and azimuth angle) are critical in both simulating SAR image from DEM data, and projecting SAR image back to DEM map. Although inaccurate sensor parameters may induce errors in the individual process, the induced errors will be canceled

out in the geometrically corrected process since these two processes are exactly opposite.

In general, the bigger of the elevation difference is, the severer of geometric distortions of SAR image will be. However, since the proposed method for CP detection is based on terrain feature, denser and more reliable tie-points are usually found in high relief areas (as illustrated in Figure 7). Therefore, the accuracy of the method is better in high elevations, and decreases in the low elevations. In order to improve the accuracy, some methods, such as SIFT [1], could be used in the flat areas. Otherwise, though SAR backscatter variations due to land covers may affect image matching, the effective outlier screening procedures developed to remove erroneous tie-points make the proposed method relatively immune to the backscatter variations in the real SAR image.

The proposed method is fully automatic, and can be implemented by the computer alone. The total processing time is about 15 mins, and the SAR image simulation and CP matching account for 35% and 56%, respectively, which means the correlation computation is time consuming and may be further accelerated through the method proposed in [12–14]. By comparing the proposed method with the

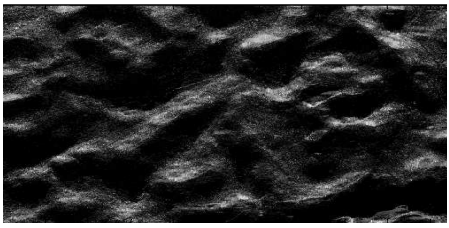

Figure 9. The geometrically corrected SAR image.

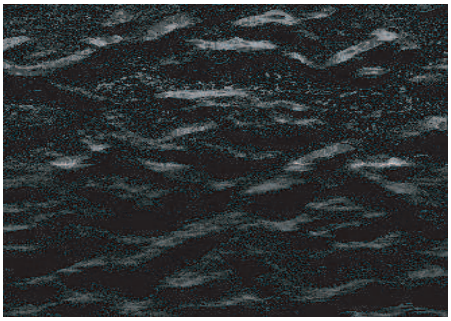

Figure 10. The mosaic image.

existed methods in [6, 9], where the TGM is the method proposed in [6] and the EBM is the method proposed in [9], we can get that the proposed method is better in accuracy and computation time.

Furthermore, in order to demonstrate the accuracy of the method, two geometrically corrected images are mosaicked. One of the images is shown in Figure 8, and the other is shown in Figure 9, which has some superposition in the range with Figure 8. To make the mosaic image look smooth, the mosaic image uses the average gray value of the two images in the overlapping regions, and directly uses the original gray value of them in the non-overlapping regions. Figure 10 shows the mosaic image, from which we can get that the mosaic result is good since the geometric accuracy of two images are both high.

4. CONCLUSION

This paper proposes a fully automated method of SAR reference image preparation for navigation. Critical technologies of the proposed method include SAR image and layover image simulation from DEM, image segmentation and clustering, outlier screening, and sub-pixel location computation. The layover image simulation provides a method to calculate the gray threshold for image segmentation. The image segmentation and clustering produces a set of denser and reliable CPs distributing along layover regions. The effective outlier screening procedure makes the proposed method relatively immune to the backscatter variations in real SAR image. The method of sub-pixel location computation makes the accurate registration between the real and simulated SAR image become reality. According to the experiments based on real data sets, the accuracy of reference image is better than 5 m. Therefore, the proposed method is accurate and effective in SAR reference image preparation under complex terrains.

In the future work, the method will be tested on other types of data sets, such as spaceborne SAR image. Furthermore, the technologies of characteristic reference image preparation, which only utilizes some characteristics of image, will also be researched.

REFERENCES

1. Ren, S., W. Chang, and X. Liu, "SAR image matching method based on improved SIFT for navigation system," *Progress In Electromagnetics Research M*, Vol. 18, 259–269, 2011.
2. Mitilineos, S. A. and S. C. A. Thompoulos, "Positioning accuracy enhancement using error modeling via a polynomial

approximation approach," *Progress In Electromagnetics Research*, Vol. 102, 49–64, 2010.

3. Konecny, G. and W. Schuhr, "Reliability of radar image data," *Proceedings of the 16th ISPRS Congress*, Tokyo, 1988.
4. Leberl, F., *Radargrammetric Image Processing*, Artech House, Norwood, Massachusetts, 1990.
5. Curlander, J. C., "Location of spaceborne SAR imagery," *IEEE Trans. Geosci. Remote Sens.*, Vol. 20, No. 3, 359–364, 1982.
6. Sheng, Y. W. and D. E. Alsdorf, "Automated georeferencing and orthorectification of amazon basin-wide SAR mosaics using SRTM DEM data," *IEEE Trans. Geosci. Remote Sens.*, Vol. 43, No. 8, 1929–1940, 2005.
7. Liu, H. X., Z. Y. Zhao, and K. C. Jezek, "Correction of positional errors and geometric distortions in topographic maps and DEMs using a rigorous SAR simulation technique," *Photogrammetric Engineering & Remote Sensing*, Vol. 70, No. 9, 1031–1042, 2004.
8. Werner, C., T. Strozzi, and U. Wegmuller, "SAR geocoding and multi-sensor image registration," *International Geosci. Remote Sens. Symposium*, Toronto, Canada, 2002.
9. Bentoutou, Y., N. Taleb, K. Kpalma, et al., "An automated image registration for application in remote sensing," *IEEE Trans. Geosci. Remote Sens.*, Vol. 43, No. 9, 2127–2137, 2005.
10. Gelautz, M., E. Mitteregger, and F. Leberl, "Automated acquisition of ground control using SAR layover and shadows," *International Geosic. Remote Sens. Symposium*, Singapore, 1997.
11. Guindon, B. and H. Maruyama, "Automated matching of real and simulated SAR imagery as a tool for round control point acquisition," *Can. J. Remote Sens.*, Vol. 12, No. 2, 621–638, 1987.
12. Mostafavi, H. and W. S. Fred., "Image correlation with geometric distortion. Part I: Acquisition performance," *IEEE Trans. Aerosp. Electron. Syst.*, Vol. 14, No. 3, 487–493, 1978.
13. Mostafavi, H. and W. S. Fred, "Image correlation with geometric distortion. Part II: Effect on local accuracy," *IEEE Trans. Aerosp. Electron. Syst.*, Vol. 14, No. 3, 494–500, 1978.
14. Franceschetti, G., M. Migliaccio, and D. Riccio, "SAR raw signal simulation of actual ground sites described in terms of sparse input data," *IEEE Trans. Geosci. Remote Sens.*, Vol. 32, No. 6, 1160–1169, 1994.
15. Zhao, Y. W., M. Zhang, and H. Chen, "An efficient ocean SAR raw signal simulation by employing fast fourier transform," *Journal of Electromagnetic Waves and Applications*, Vol. 24,

No. 16, 2273–2284, 2010.

16. Chang, Y.-L., C.-Y. Chiang, and K.-S. Chen, "SAR image simulation with application to target recognition, *Progress In Electromagnetics Research*, Vol. 119, 35–57, 2011.
17. Hiroshi, K. and L. Tetsuji, "Automated matching of real and simulated SAR imagery for geometric correction," *10th Annal International Geoscience and Remote Sensing Symposium*, Washington D.C., Maryland, 1990.
18. Rees, W. G. and A. M. Steel, "Simplified radar mapping equations for terrain correction of space-borne SAR images," *Int. J. Remote Sens.*, Vol. 22, No. 18, 3643–3649, 2001.
19. Femand, M., "Topographic distance and watershed lines," *Signal Processing*, Vol. 38, 113–125, 1994.
20. Otsu, N., "A threshold selection method from gray-level histograms," *IEEE Trans. Systems, Man, and Cybemetics*, Vol. 9, No. 1, 62–66, 1979.
21. Qi, F., V. Tavakol, D. Schreurs, and B. K. J. C. Nauwelaers, "Discussion on validity of hadamard speckle contrast reduction in coherent imaging systems," *Progress In Electromagnetics Research*, Vol. 104, 125–143, 2010.
22. Bentoutou, Y., N. Taleb, M. Chikr, et al., "An invariant approach for image registration in digital subtraction angiography," *Pattern Recognit.*, Vol. 35, No. 12, 2853–2865, 2002.
23. Tran, L. V. and J. Sklansky, "Flexible mask subtraction for digital angiography," *IEEE Trans. Med. Imag.*, Vol. 35, No. 2, 220–223, 1992.
24. Bayer, T., R. Winter, and G. Schreier, "Terrain influences in SAR backscatter and attempts to their correction," *IEEE Trans. Geosci. Remote Sens.*, Vol. 29, No. 3, 451–462, 1991.